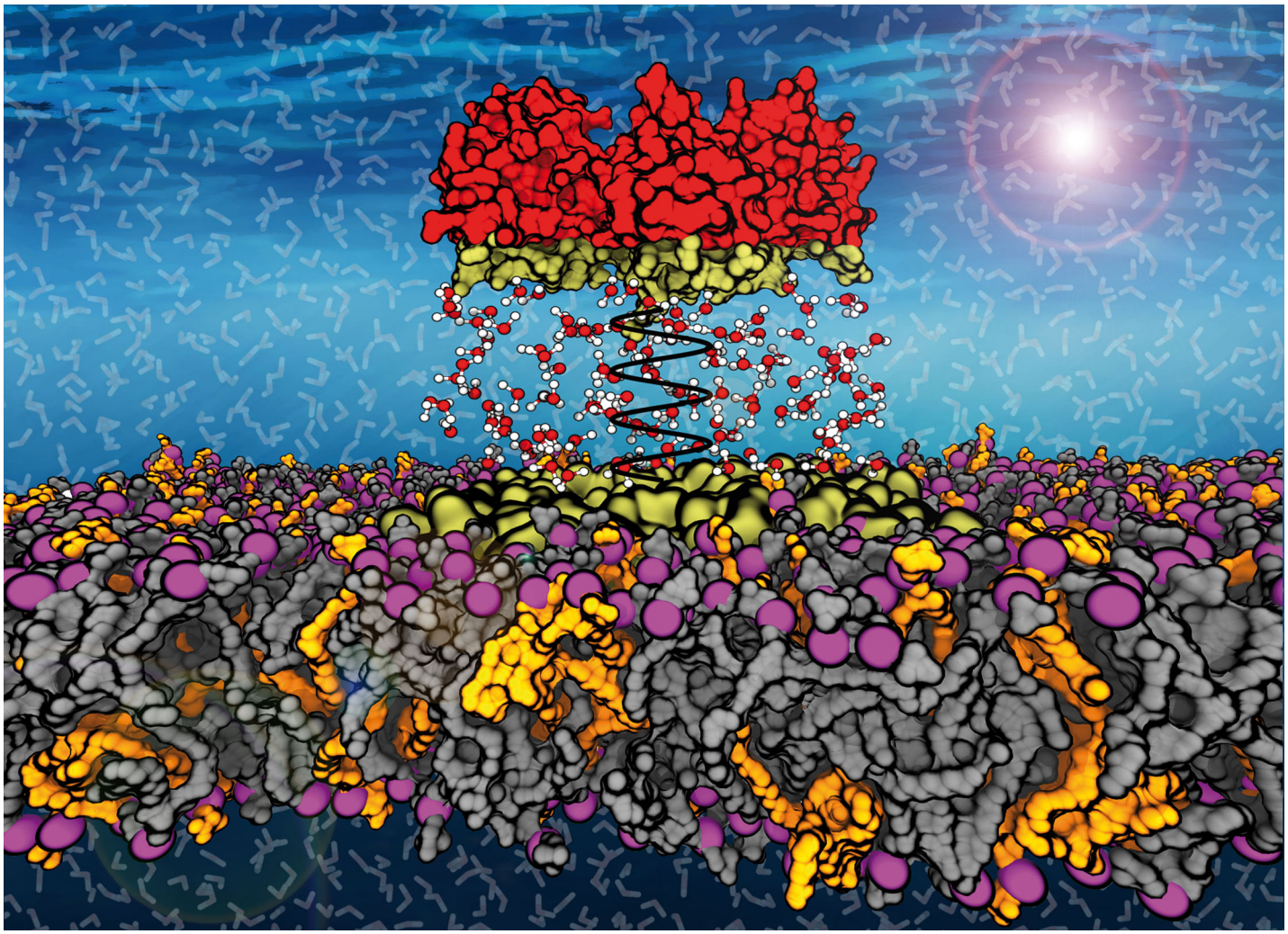

Showcasing research from the Groups of Prof. Lars V. Schäfer at Ruhr University Bochum, Germany, and Prof. Matthias Heyden at Arizona State University, USA

Atomistic characterization of collective protein–water–membrane dynamics

This work uses atomistic molecular dynamics simulations to study how water mediates correlated vibrational motion between the surface atoms of a protein and a membrane bilayer. For protein–membrane distances of up to 25 Å, the properties of propagating collective modes in the hydrogen bond network of separating hydration layers are found to be affected by combined interactions with both surfaces, while simultaneously non-zero correlations of protein and lipid surface atom vibrations are observed.

As featured in:

See Lars V. Schäfer, Matthias Heyden *et al.*, *Phys. Chem. Chem. Phys.*, 2019, **21**, 15958.

ROYAL SOCIETY OF CHEMISTRY | Celebrating IYPT 2019

rsc.li/pccp

Registered charity number: 207890

PCCP

PAPER

View Article Online
View Journal | View Issue

Cite this: *Phys. Chem. Chem. Phys.*, 2019, **21**, 15958

Received 15th February 2019,
Accepted 13th April 2019

DOI: 10.1039/c9cp00725c

rsc.li/pccp

Atomistic characterization of collective protein–water–membrane dynamics†

Christopher Päslack,[a] Lars V. Schäfer *[a] and Matthias Heyden *[b]

Correlated vibrational motion on the sub-picosecond timescale and associated collective dynamics in a protein–membrane environment are characterized using molecular dynamics simulations. We specifically analyze correlated motion of a membrane-associated protein and a lipid bilayer for distinct separation distances. Correlated vibrations persist up to distances of 25 Å between both biomolecular surfaces. These correlations are mediated by separating layers of water molecules, whose collective properties are altered by the simultaneous presence of protein and lipid bilayer interfaces.

1 Introduction

Biomolecules in cells are tightly packed in the cytoplasm with molecular surfaces separated by distances on the order of 10 Å. This remaining space is filled by the aqueous solvent matrix in which many biomolecular processes take place.[1] Recent experimental and theoretical studies focused on mechanisms that determine the structure and dynamics of proteins and reveal how protein and solvent dynamics affect each other.[2–7] The structure and dynamics of water in the hydration shell of proteins differs from bulk water. Especially in the first hydration shell, diffusional and rotational dynamics of water molecules are slowed down, which is closely related to increased hydrogen bond (HB) lifetimes and shifted frequencies of intermolecular vibrations.[8–13] Hydration water contributes to the stability of biomolecular structures and mediates interactions relevant for molecular recognition.[14–16] Further, dewetting events are required to form intermolecular contacts and affect binding kinetics.[17–19]

Collective motions in proteins cover a broad range of timescales. They were first investigated by normal mode analysis and linked to low-frequency modes in the density of states of proteins *via* incoherent neutron scattering.[20,21] A study by Hong *et al.* revealed how specific, collective in-phase dynamic modes can facilitate access for substrates to the binding site of cytochrome P450cam.[22] Further, simulations have characterized collective modes that propagate from the surface of a protein into its hydration shell.[23–27] Despite this body of knowledge on protein solutions[28–30] and the biological significance of membranes,[31–33] collective protein–lipid dynamics – and how they are mediated by hydration water – have not yet been investigated.

Here, we characterized correlated low-frequency vibrations between the membrane-associated protein annexin B12 (Anx) and a lipid bilayer consisting of a 7 : 3 mixture of DOPC and DOPS lipids (Fig. 1). We further analyzed correlated vibrations of protein and lipid atoms with water separating both biomolecular surfaces. Atomic vibrations were sampled in all-atom molecular dynamics (MD) simulations and their correlations were analyzed for membrane-bound and unbound states. This analysis revealed the persistence of correlated vibrations between atoms of the Anx protein and membrane lipids up to 25 Å separation distances, which are mediated by the separating shell of hydration water. This finding is supported by the observation of simultaneous modifications of collective protein–water and lipid–water dynamics, which describe the propagation of collective modes from the protein and lipid bilayer surfaces into water layers separating both. A complementary analysis in the time-domain provides an estimate for the exchange of information with respect to the average thermal energy *via* the collective modes described here.

2 Methods

2.1 Simulation protocol

The peripheral membrane protein annexin B12 (Anx) was used as a model for a membrane-associating protein. For the membrane, we used a lipid bilayer consisting of a 7 : 3 mixture of DOPC and DOPS lipids with a total of 512 lipids (256 lipids in each leaflet). We started from an X-ray crystal structure of Anx

[a] *Center for Theoretical Chemistry, Faculty of Chemistry and Biochemistry, Ruhr-University Bochum, D-44780 Bochum, Germany. E-mail: lars.schaefer@ruhr-uni-bochum.de; Fax: +49 234 3214045; Tel: +49 234 3221582*

[b] *School of Molecular Sciences, Arizona State University, Tempe, AZ 85287-1604, USA. E-mail: heyden@asu.edu; Tel: +1 480 965-3980*

† Electronic supplementary information (ESI) available: Simulation protocol, details on analysis of correlated motions. See DOI: 10.1039/c9cp00725c

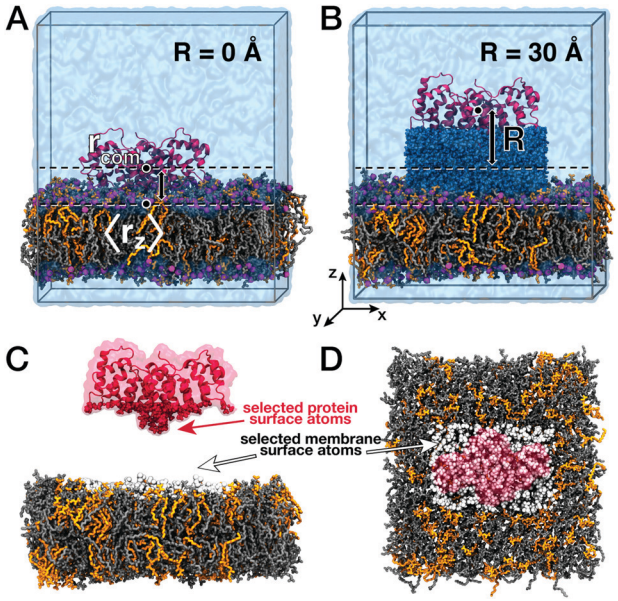

Fig. 1 Annexin B12 on a phospholipid bilayer. Starting structures for MD simulations were generated with Anx (red) positioned at various distances R from the bilayer (DOPC: gray, DOPS: orange). (A) Protein–lipid distance R = 0 Å (Anx bound to the lipid bilayer). (B) Protein–lipid distance R = 30 Å (interfacial water between protein and membrane shown in dark blue). (C and D) Surface non-hydrogen atoms selected for the cross-correlation analysis. Anx atoms were selected on the membrane-facing side (red) and membrane atoms were selected in a rectangular area of similar size as the protein cross section (white).

(PDB ID code 1DM5)[34] and from a pre-equilibrated lipid bilayer.[35] The simulated systems were prepared following a protocol described in previous work,[11] where the initial position of the protein bound to the lipid bilayer was chosen according to experimental data.[36]

The protein and bilayer were placed in a rectangular box with a size of approximately 135 × 135 × 157 Å^3 containing *ca.* 64 000 water molecules. The net charge of the system was neutralized with Na^+ and Cl^- ions. Periodic boundary conditions were applied in all three dimensions. The MD simulations were carried out using GROMACS 5.0.6[37] with the Amber ff99SB*-ILDNP force-field[38–41] for Anx and the all-atom Slipids force-field[35,42] for the lipids. The TIP4P/2005 model[43] was used for water.

We employed the SETTLE and LINCS algorithms[44,45] to constrain the internal degrees of freedom of water molecules and the bonds in other molecules, respectively, allowing to integrate the equations of motion with time steps of 2 fs. Short-range non-bonded Coulomb and Lennard-Jones 6,12 interactions were treated with a Verlet buffered pair list[46] with potentials smoothly shifted to zero at a 10 Å cut-off. Long-range Coulomb interactions were treated using the smooth particle mesh Ewald (PME) scheme[47,48] with a grid spacing of 1.2 Å and cubic spline interpolation. Analytical dispersion corrections were applied for energy and pressure to account for the truncation of the Lennard-Jones interactions.

After an initial energy minimization (500 steps steepest decent) of the Anx protein and the DOPC/DOPS bilayer, the protein and two bound Ca^{2+} ions were translated along the z-axis (*i.e.*, the direction normal to the membrane) to generate configurations in which Anx is located at various distances R to the bilayer, covering an R-range from 0 to 32 Å. Each of the systems was then solvated with water. Sodium and chloride ions were included at physiological concentrations *via* substitution of randomly selected water molecules. Care was taken not to introduce water molecules in the hydrophobic part of the bilayer. After a second energy minimization (500 steps steepest decent), the systems were equilibrated for 5 ns in the isothermal–isobaric (*NPT*) ensemble with harmonic position restraining potentials applied to the heavy atoms of the protein (force constants 1000 kJ mol^{-1} nm^{-2}). The temperature was kept at 298 K by a velocity-rescaling thermostat[49] with a coupling time constant of 0.1 ps. For simulations at constant 1.0 bar pressure, a semi-isotropic Berendsen barostat[50] with a coupling time constant of 0.5 ps and a compressibility of 4.5 × 10^{-5} bar^{-1} was applied, with lateral (xy) and normal (z) dimensions of the simulation box coupled separately.

For each configuration generated with a specific protein–membrane distance R, simulations of 100 ns were performed in the *NPT* ensemble. During the equilibrations (but not the production simulations, see below), two harmonic restraining potentials were applied to the angle between the z-axis and the connecting vectors between the C_α-atoms of (1) residues Ser35/Val195 and (2) residues Glu138/His254 (force constant 200 kJ mol^{-1} rad^{-2}). This was required to avoid overall tumbling of the protein during the simulations. In addition, a harmonic umbrella potential with a force constant of 1500 kJ mol^{-1} nm^{-2} was applied in the z-direction between the centers of mass of Anx and selected phosphorus atoms in the lipid head groups of the upper leaflet. The phosphorus atoms were selected in a cylindrical geometry with an inner radius of r_0 = 30 Å and an outer radius of r_1 = 35 Å, where weighted contributions to the center of mass position were switched to 0 between r_0 and r_1. The harmonic restraint between the centers of mass of the protein and the phosphorus atoms in the defined cylindrical region kept the protein at the selected distance from the lipid bilayer.

After the 100 ns equilibrations, the *NPT* equilibrations were extended by another 5 ns for each distance with a stronger angle restraint (1000 kJ mol^{-1} rad^{-2}) to enforce an ideal orientation of the protein, such that the bottom surface of Anx was parallel to the membrane surface (Fig. 1).

Finally, for selected distances (R = 0 to 30 Å, in 5 Å steps, and two additional distances of 28 Å and 32 Å), we carried out 20 independent 100 ps simulations in the *NVE* ensemble for analysis of collective motions. The starting structures for the *NVE* simulations were taken from the final 2 ns of the above *NPT* equilibrations, separated by 100 ps. Atom positions and velocities were recorded every 8 fs for vibrational analysis. The production simulations in the *NVE* ensemble were entirely unbiased, *i.e.*, without umbrella potentials or angle restraints, to avoid artifacts in the time-correlation functions and their Fourier transforms due to the restraining potentials. The mass density profiles along the membrane normal (Fig. S1), as well as the analysis of the stability of protein orientation (Fig. S2) and position (Fig. S3 and S4) with respect to the bilayer are provided in the ESI.†

2.2 Velocity cross-correlation spectra

Collective vibrations in the protein–membrane system were analyzed using a generalized vibrational density of states (VDOS),

$$I(\omega, r_i, r_j) = \int e^{-i\omega t} \langle \tilde{v}_i(\tau, r_i) \cdot \tilde{v}_j(\tau + t, r_j) \rangle_\tau dt \quad (1)$$

which includes correlated velocity fluctuations of distinct particles $i \neq j$ at their respective positions r_i and r_j (see ref. 24 and ESI†). In eqn (1), atomic velocities $\tilde{v} = \sqrt{m}v$ are weighted by the square-root of the atom mass yielding an expression for the average thermal energy for auto-correlations $i = j$. The brackets $\langle \ldots \rangle_\tau$ denote ensemble-averaged time-correlation functions with reference times τ. Eqn (1) allows for direct evaluation of correlated vibrational motion between protein and membrane surface atoms. Here, we restrict the analysis to non-hydrogen atoms, which dominate the vibrational spectra at far-infrared frequencies below 400 cm^{-1}.

In addition to correlated protein–membrane vibrations, we analyzed protein–water and membrane–water correlated vibrations involving water molecules located in the space between Anx and the lipid bilayer. We computed cross-correlation spectra including water oxygens sampled at various distances to the protein or membrane surface, ranging from 2.5–10.0 Å with increments of 0.5 Å. Explicit atomic velocities were replaced by localized velocity densities,

$$\rho_{\tilde{v}_i}(r) \approx \sum_i \tilde{v}_i \frac{1}{(2\pi\sigma^2)^{3/2}} e^{-(|r_i - r|^2/2\sigma^2)} \quad (2)$$

for water oxygens to obtain well-defined correlation functions for each distance r to the protein or membrane surface.[51] The localized velocity densities defined by the Gaussian kernel (σ = 0.4 Å) are dominated by contributions from the closest atom at all times. The density $\rho_{\tilde{v}_i}$ was sampled at points evenly distributed around the protein/membrane surface at selected distances to the closest non-hydrogen atom (see ref. 24 and Fig. S5 in the ESI†). Protein–water and membrane–water correlated vibrations were analyzed *via* the following expression,

$$I(\omega, r_{S,OW}) = \int e^{i\omega t} \langle \tilde{v}_S(\tau, r_S) \rho_{\tilde{v},OW}(\tau + t, r_{OW}) \rangle_\tau dt \quad (3)$$

where subscripts S and OW refer to solute (protein or membrane) non-hydrogen atoms and water oxygen atoms, respectively; $r_{S,OW} = |r_S - r_{OW}|$ describes the distance between density sampling points and the solute atom. For every velocity density sampling point, the time cross-correlation with the velocity of the closest non-hydrogen solute atom was analyzed to obtain the spectrum of correlated vibrational motion. Spectra of distance-dependent ($r_{S,OW}$) correlated solute–solvent vibrations were computed for varying protein–membrane distances R. We focus our analysis on the longitudinal components of the velocity vectors, whose collective dynamics are related to sound propagation.[24,26] The time-symmetry of ensemble-averaged cross-correlation functions at equilibrium allows distinguishing positive and negative intensities in the resulting spectra, which correspond to parallel and antiparallel vibrations of correlated velocity vectors at a given frequency, respectively.

We visualize correlation spectra obtained as a function of the real-space distance using the inverse distance $k = 2\pi/r_{S,OW}$, in analogy to coherent scattering data. We identify dispersive collective modes propagating with a wave velocity $v_{mode} = d\omega/dk$. The k-resolved spectra, recorded for distinct protein–membrane separations R, are directly related to longitudinal density current spectra $I_J^{\parallel}(k,\omega) = (\omega^2/k^2)S(k,\omega)$, which describe correlated density fluctuations *via* the experimentally accessible dynamic structure factor $S(k,\omega)$.

3 Results and discussion

3.1 Collective protein–membrane vibrations

First, we assessed correlated motion between the protein and the lipid bilayer. We analyzed the evolution of the cross-correlation spectra $I(\omega,r_i,r_j)$ between non-hydrogen atoms of the protein (index i) and the lipids (index j), each selected at the corresponding interface (see Fig. 1C and D) with increasing protein–membrane distance R. For each separation distance R, we obtained $I(\omega,R)$ shown in Fig. 2A by averaging over individual pair-wise cross-correlations. Protein and membrane surface atoms were partitioned into slabs (Δx = 5 Å, Δy = 5 Å) within which the cross-correlations were analyzed to ensure alignment of the vectors $r_j - r_i$ with the membrane normal. The most prominent feature in all spectra $I(\omega,R)$ is the positive-intensity peak at low frequencies $\omega < 25$ cm^{-1}, describing an in-phase oscillation of membrane and protein atoms along the connecting vector. As R increases, the peak is shifted toward zero frequencies. Additionally, a negative-intensity mode is observed at 30–120 cm^{-1}, which describes anti-phase motion of protein and membrane atoms. This peak is broad at short distances and becomes narrow at larger distances. The amplitude of correlated vibrations of protein and lipid atoms remains detectable above the noise level for separation distances R of up to 25 Å (inset Fig. 2). For $R \geq 30$ Å it is no longer possible to distinguish between correlated vibrations and statistical noise, demonstrating that correlations at smaller separation distances are not caused by finite-size effects. The negative-intensity mode is dispersive: its frequency decreases monotonically for increasing protein–membrane separations R resulting in a frequency shift of 67 cm^{-1} from 25 Å to 0 Å. For direct protein–membrane contact (R = 0 Å), the negative signal has a pronounced high-frequency tail, which we attribute to intermolecular vibrations between directly interacting protein and lipid groups.

The results shown in Fig. 2A report on correlated vibrations between atoms of the protein and membrane surfaces. To investigate the propagation of collective modes, *i.e.*, correlated vibrational motion between the lipid and protein surfaces analyzed in Fig. 2A into the interior of the protein, we repeated the analysis using mass-weighted atomic velocities of atoms selected within a hemisphere (oriented towards the membrane-facing protein surface) of 10 Å radius around the protein center of mass. The results are shown in Fig. 2B and indicate a decreased overall intensity of the correlations, as expected due to the increased separation distance between the membrane surface

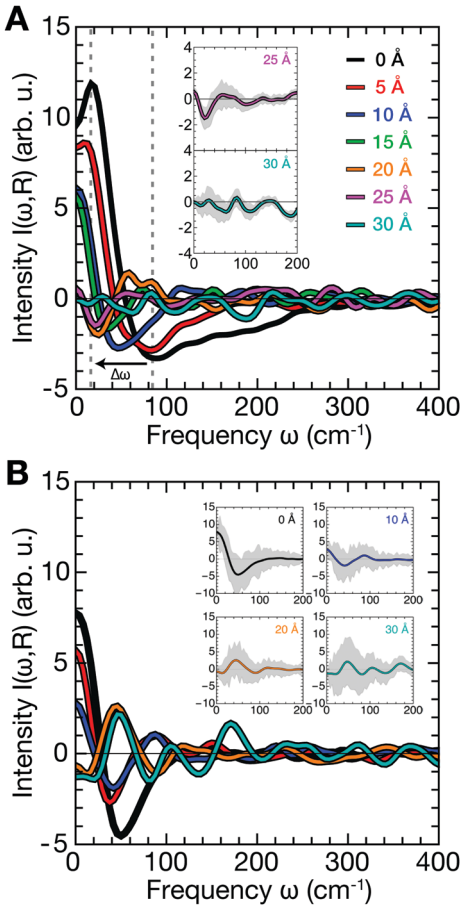

Fig. 2 (A) Protein–membrane cross-correlation spectra $I(\omega,R)$ for different separation distances R between the molecular surfaces. The frequency change $\Delta\omega \approx 67$ cm^{-1} for the negative-intensity peak is highlighted with gray dashed lines and an arrow. (B) Cross-correlation spectra $I(\omega,R)$ between atoms of the membrane surface and atoms within the core of the Anx protein (in contrast to atoms at the binding interface) computed at different separation distances R between the two molecular surfaces. In both panels, the insets show the standard error from 20 individual simulations as gray areas for selected protein–membrane separation distances. Each spectrum was smoothed with a 10 cm^{-1} Gaussian window function.

and the protein core in comparison to the separation between the binding interfaces. In addition, Fig. 2B shows that the correlation intensities decrease significantly faster with increasing R. Relative to the cross-correlation spectrum for R = 0 Å, both, the positive and negative peak intensities (apart from the dispersive shift in frequency) decrease to just 40% of their initial intensity for R = 10 Å in Fig. 2B. When intensities in the cross-correlation spectra are compared between membrane and protein surface atoms for R = 0 Å and R = 10 Å in Fig. 2A, the positive peak decreases only to approximately 50% of its original intensity, while the negative intensity even retains roughly 80%. Correlated vibrations between the protein core and the membrane surface are therefore more sensitive to the separation between both binding interfaces. Hence, collective modes that propagate through the HB network of water separating the protein and membrane surfaces seem to dissipate more efficiently within the protein.

3.2 Collective protein–water and membrane–water vibrations

Next, we analyzed protein–water and membrane–water correlations. As a reference, we first computed k-resolved protein–water and membrane–water cross-correlation spectra according to eqn (3) for simulations of Anx in water (no membrane) and the membrane in water (no protein) as shown in Fig. 3, which effectively represents an infinite protein–membrane separation distance R. The selection of surface atoms was the same as shown in Fig. 1C and D and velocity densities for water oxygens were sampled at distances to the selected protein or membrane surface atoms in the range from 2.5–10.0 Å. Compared to the protein, the overall correlation intensity is weaker for the membrane by approximately a factor of 2. Both systems have two distinct modes that dominate the spectra: (1) a dispersive high-frequency mode with negative intensity and (2) a low-frequency mode with positive intensity. In the high k/short distance (~3 Å, first hydration layer) limit, the signals correspond to peaks found in the VDOS of water and exhibit their largest magnitude, describing intermolecular vibrations such as HB bending (<100 cm^{-1}) and stretching modes (~200 cm^{-1}). The signals at smaller k/longer distances (>3 Å) correspond to collective modes that propagate through the water HB network. The dispersion relation $d\omega/dk$ of the negative-intensity peak (Fig. 3, dashed lines) in the linear regime yields wave propagation velocities of 2313 ± 77 m s^{-1} for Anx and 1870 ± 128 m s^{-1} for the DOPC/DOPS bilayer.

3.3 Distance-dependence of wave velocities

Analogous to the analysis in Fig. 3, longitudinal collective protein–water and membrane–water vibrations were also analyzed from k-resolved cross-correlation spectra obtained from simulations including both the protein and the membrane at varying separation distances R. As shown in Fig. 1B, the water molecules considered here are located in between the protein and membrane. Applying the dispersion relation for the protein–membrane systems, we obtain wave propagation velocities from protein–water and

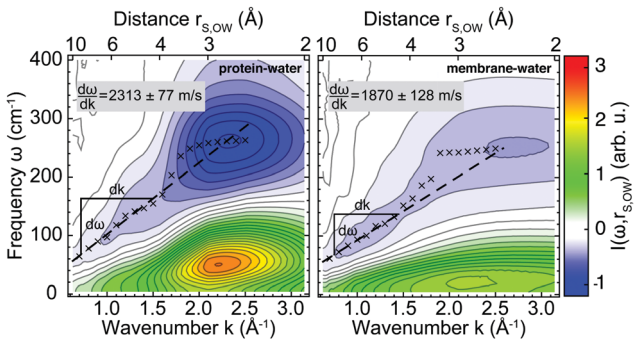

Fig. 3 Cross-correlation spectra of mass-weighted atomic velocities and localized velocity densities (eqn (3)) for vibrations of non-hydrogen protein or membrane surface atoms with hydration water oxygen atoms as a function of reciprocal distance $k = 2\pi/r_{S,OW}$. Shown are results for Anx in water (left panel; without a lipid bilayer) and for a DOPC/DOPS bilayer (right panel; without a protein). Crosses trace the peak-intensity of the negative-intensity modes for which linear dispersion curves (dashed lines) were determined.

membrane–water cross-correlation spectra at varying protein–membrane distances as shown in Fig. 4. Notably, the observed propagation velocities of the analyzed collective modes v_{mode} are increased significantly in both cases for separation distances $R < 25$ Å between protein and membrane. While this increase only amounts to 10% in case of the protein–water collective modes, the propagation velocities are increased by 40% for collective membrane–water modes. The data in Fig. 4 demonstrate a sharp modulation of the mode velocities in a narrow distance range (between R = 25–28 Å) corresponding to the thickness of a single hydration shell. Reassuringly, the mode velocities for the largest studied separation distances converge to the values at infinite separation distance as reported in Fig. 3.

The maximum change Δv_{mode} is about +927 m s^{-1} for the lipid bilayer and +307 m s^{-1} for Anx. The propagation of collective modes involving the lipid bilayer and its hydration water becomes similar to fast sound in bulk water ($\approx$3000 m s^{-1}).[52,53] However, we do not observe a strictly monotonous trend for neither protein nor lipid bilayer besides the increase for distances $R < 25$ Å, which coincides with the gradually increasing overlap of the protein and membrane hydration shells. The inset of Fig. 4 shows that the protein surface is not planar and its hydration shell has a conical shape. Assuming a 10 Å thickness of the hydration layer, there is almost no overlap of the protein and membrane hydration shells at a separation distance of R = 30 Å. However, at 25 Å distance the hydration shells begin to partially overlap. When the protein binds to the membrane, *i.e.*, for short distances, the protein and lipids share one single hydration shell. Single particle dynamics, such as water self-diffusion and rotational relaxation, are slowed down in the hydration shell and the hydrogen bond network becomes effectively more rigid.[6,11,54,55] This is correlated to changes in local thermodynamic properties as observed in our previous work,[11] but the effects are short-ranged and mainly affect a single hydration layer within distances of 3–5 Å. However, here we analyze collective modes involving protein and membrane surface atoms and surrounding water molecules, which tend to extend over distances of at least 10 Å as observed in Fig. 3 and in previous studies on protein–water systems.[24,26]

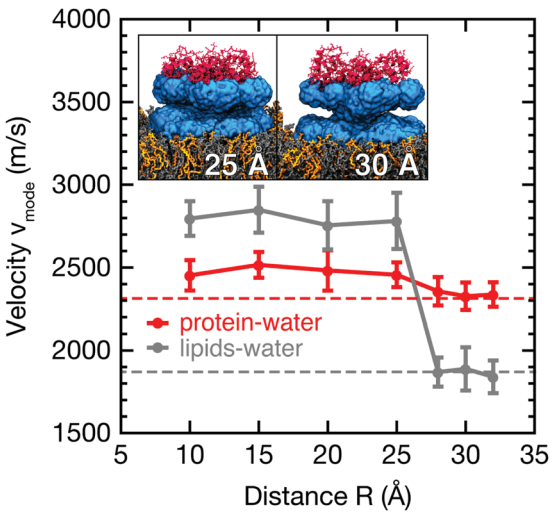

Fig. 4 Wave propagation velocities of longitudinal, collective protein–water (red) and membrane–water (gray) modes for distinct protein–membrane separation distances R (see Fig. S6 in the ESI† for corresponding cross-correlation spectra). Error bars show standard errors of the mean from 20 individual simulations. Dashed lines indicate reference values for Anx in water (no membrane) and the lipid bilayer in water (no protein); insets visualize the onset of overlapping protein and membrane hydration layers of 10 Å thickness.

In addition to these previous observations, we observe that the presence of two biomolecular surfaces with separation distances of 25 Å or less modifies collective protein–water and membrane–water dynamics and results in the onset of correlated motion of protein and lipid atoms. Our observations can be compared to abrupt dynamical transitions in water hydrogen bond network dynamics for crowded protein solutions observed experimentally for protein–protein distances of 30–40 Å and 20–25 Å in accompanying simulations.[56] Indeed, the increased propagation velocity of protein–water and membrane–water collective modes for separation distances $R < 25$ Å may serve as a sensitive indicator of long-lived water hydrogen bond networks connecting both biomolecular surfaces, which are likely to feature collective properties similar to low-temperature water or ice.[57,58]

To support this assumption, the lifetimes of water–water hydrogen bonds involving the water molecules between the protein and the membrane (see Fig. 1B, dark blue) were analyzed. As described in the ESI,† we computed the hydrogen bond correlation functions $C_{HB}(t)$ and estimated the HB lifetimes τ_{HB} as $C_{HB}(\tau_{HB}) = 1/e$. The average lifetimes for all water molecules between the protein and the membrane are shown in Fig. 5A.

For short protein–membrane distances $R \leq 10$ Å, the average lifetimes deviate strongly from the bulk lifetime of about 3 ps. Water molecules are confined and H-bonds persist on average up to almost 20 ps, *i.e.*, almost one order of magnitude longer than in bulk. For increasing distances R, the correlation times drop to almost the bulk lifetime, however, not reaching the bulk value since water molecules in the first hydration shells are still included in the average. These findings agree with previous results from two-dimensional infrared spectroscopy and MD simulations,[56] where a dynamic transition of HB lifetimes of water molecules between proteins in crowded solutions occurred for comparable separation distances between protein surfaces. In addition, we analyzed the average HB lifetimes involving water molecules selected as a function of distance from either the protein or membrane surface (Fig. 5B, top and bottom panels, respectively); these analyses were carried out for simulations with varying protein–membrane distances R. Notably, only at protein–membrane distances of $R \geq 25$ Å, *i.e.*, in the center between protein and membrane, the dynamics of water become similar to bulk, marking the onset of overlapping solvation shells. These results corroborate the interpretation of shifted mode velocities v_{mode} (Fig. 4) due to hydration shell overlap. Notably, collective modes with a propagation velocity of 2500 m s^{-1} traverse a 25 Å separation distance between the protein and the membrane in just 1 ps.

The observation that correlated vibrations between the protein and membrane persist up to 25 Å separation distance may have important implications for crowded environments

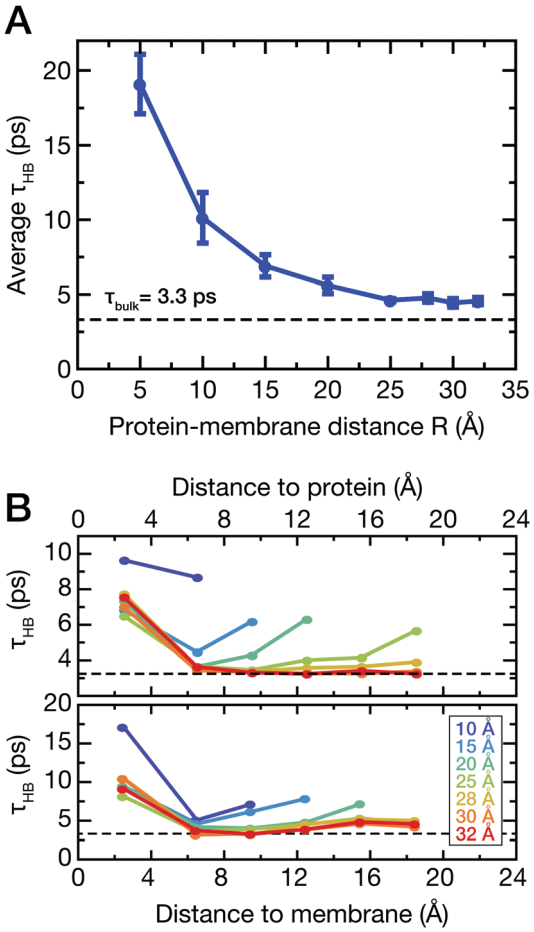

Fig. 5 Hydrogen bond lifetimes τ_{HB} of water. (A) Average hydrogen bond lifetimes involving water molecules between the membrane and the membrane-facing side of Anx. The data are shown as a function of protein–membrane distance R. Error bars depict standard deviations from individual *NVE* simulations for each distance R. (B) Hydrogen bond lifetimes of water molecules at different distances to the protein (top panel) and membrane (bottom panel) surfaces, respectively. The analysis was carried out for simulations with distinct protein–membrane distances R.

such as the cytoplasm. The wave velocities of protein–water and membrane–water collective modes are affected by the combined influence of both biomolecular surfaces. Importantly, the presence of a protein substantially increases the propagation velocities obtained from membrane–water cross-correlation spectra, in this respect resembling fast sound-like dynamics as observed in solid forms of water with slow structural relaxation times. However, the propagation velocities of protein–water collective vibrations are enhanced to a much smaller extent upon hydration shell overlap. While the protein–water collective vibrations propagate inherently faster than the membrane–water vibrations in the infinite dilution limit, membrane–water collective vibrations exhibit faster propagation velocities for protein-membrane separation distances $R < 25$.

3.4 Time-domain analysis of correlated motions

To complement our analysis of correlated vibrational motion *vs.* frequency shown in Fig. 2 and 3, we provide the corresponding time-resolved cross-correlations in Fig. 6. The latter are normalized by the corresponding average auto-correlations of protein or lipid atoms at zero correlation time, which correspond to the product of the particle mass and the squared velocity component along the vector separating the cross-correlated atoms. This normalization allows one to interpret cross-correlation intensities in terms of fractions of the average thermal energy per degree of freedom exchanged between particles.

The peak intensities of the cross-correlation functions indicate that, in this single degree of freedom, correlated particles exchange between 0.25% and 1% of their energy with each other on a 50 fs timescale. Since our simulations are carried out under equilibrium conditions, no net flow of energy takes place. However, the amount of exchanged energy can be interpreted in terms of dynamic information relative to the thermal fluctuations.

Further, we follow the peak intensities of the time-resolved cross-correlation functions for distinct separation distances in Fig. 7, which describe the spatial dissipation of this dynamic information. While the maximum peak intensities observed at the shortest correlation distances, *i.e.*, for particles in direct contact with each other, are only about 1% of the thermal energy, we note that the exchange of dynamic information and its propagation to larger distances is very fast (*ca.* 10–100 fs), as seen from the position of the peaks in Fig. 6. Therefore, the

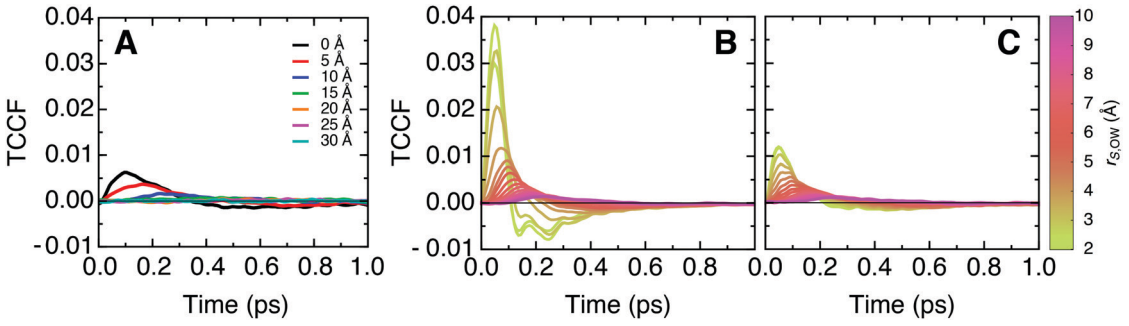

Fig. 6 Time domain representation of the longitudinal mass-weighted velocity cross-correlation functions (TCCF) between (A) protein–membrane, (B) protein–water, and (C) membrane–water atoms for distinct separation distances. The data correspond to the inverse Fourier transform of the frequency spectra shown in Fig. 2A and 3. The cross-correlation functions are normalized by the value of the corresponding mass-weighted velocity time auto-correlation function at t = 0, which describes the thermal energy per degree of freedom at the simulation temperature.

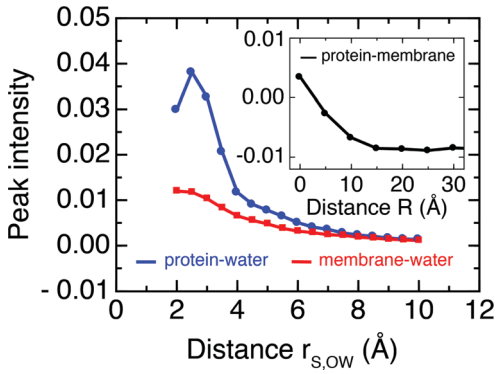

Fig. 7 Peak intensity of mass-weighted velocity time cross correlation functions between protein–membrane atoms (black, inset) and protein–water (blue) and membrane–water atoms (red) as a function of separation distance. Numerical values are equivalent to the *y*-axis scales in Fig. 6 and describe fractions of the average thermal energy per degree of freedom.

amount of energy exchanged between particles quickly accumulates on picosecond timescales.

4 Conclusions

The correlated vibrational motion of Anx, the lipid bilayer and the separating layers of hydration water may affect the kinetics of binding of the protein to the membrane surface. The expulsion of the last separating hydration water layers between binding interfaces is observed as a collective dewetting transition in simplified hydrophobic model systems[17] and creates a kinetic barrier, which can be characterized as a peak in the friction profile along the binding coordinate. While the models, for which this behavior has been studied in detail, lack the chemical heterogeneity and flexibility of a realistic biomolecular surface, enhanced water density fluctuations and transient dewetting can be observed for hydrophobic protein surface patches in more realistic simulation models.[59] We speculate that collective dewetting transitions may be influenced by the correlated vibrations between atoms in both binding interfaces, mediated through the separating water molecules as observed in this study. The intensities of membrane–water correlated vibrations are weaker than those for the protein and water. A reason may be that a lipid bilayer possesses a large variety of collective dynamics spanning timescales from 10^{-4}–10^{-10} s, where a large number of vibrational modes fall into the ns-regime of peristaltic and undulatory oscillations.[60] Finally, our results corroborate the idea of hydration water-mediated collective motion between biomolecular interfaces over length scales of >10 Å. This may be of key importance in crowded cellular environments, where average distances between neighboring biomolecular surfaces are frequently on the order of $\sim$10 Å. Changes in single-particle dynamics such as self-diffusion and rotational reorientation of water molecules are typically restricted to the first hydration shell, while collective protein–water dynamics persist up to $\sim$10 Å. Our findings provide evidence for the mediation of correlated motion between biomolecular surfaces by a dynamic hydration shell, which features modified characteristics of membrane–water and protein–water correlated vibrations.

Conflicts of interest

There are no conflicts to declare.

Acknowledgements

The Steinbuch Centre for Computing (SCC), Karlsruhe/Germany, is acknowledged for providing computational resources. This work was funded by the Deutsche Forschungsgemeinschaft (DFG, German Research Foundation) under Germany's Excellence Strategy – EXC-2033 – project number 390677874 and an Emmy-Noether grant (SCHA 1574/3-1) to L. V. S.

References

1 P. Ball, *Proc. Natl. Acad. Sci. U. S. A.*, 2017, **114**, 13327–13335.
2 Y. Levy and J. N. Onuchic, *Annu. Rev. Biophys. Biomol. Struct.*, 2006, **35**, 389–415.
3 S. Ebbinghaus, S. J. Kim, M. Heyden, X. Yu, U. Heugen, M. Gruebele, D. M. Leitner and M. Havenith, *Proc. Natl. Acad. Sci. U. S. A.*, 2007, **104**, 20749–20752.
4 L. Hong, X. Cheng, D. C. Glass and J. C. Smith, *Phys. Rev. Lett.*, 2012, **108**, 238102.
5 V. Conti Nibali and M. Havenith, *J. Am. Chem. Soc.*, 2014, **136**, 12800–12807.
6 A. C. Fogarty and D. Laage, *J. Phys. Chem. B*, 2014, **118**, 7715–7729.
7 G. Schirò, Y. Fichou, F.-X. Gallat, K. Wood, F. Gabel, M. Moulin, M. Härtlein, M. Heyden, J.-P. Colletier, A. Orecchini, A. Paciaroni, J. Wuttke, D. J. Tobias and M. Weik, *Nat. Commun.*, 2015, **6**, 6490.
8 B. Bagchi, *Chem. Rev.*, 2005, **105**, 3197–3219.
9 A. R. Bizzarri and S. Cannistraro, *J. Phys. Chem. B*, 2002, **106**, 6617–6633.
10 M. Heyden and M. Havenith, *Methods*, 2010, **52**, 74–83.
11 O. Fisette, C. Päslack, R. Barnes, J. M. Isas, R. Langen, M. Heyden, S. Han and L. V. Schäfer, *J. Am. Chem. Soc.*, 2016, **138**, 11526–11535.
12 A. Debnath, B. Mukherjee, K. Ayappa, P. K. Maiti and S.-T. Lin, *J. Chem. Phys.*, 2010, **133**, 174704.
13 R. A. X. Persson, V. Pattni, A. Singh, S. M. Kast and M. Heyden, *J. Chem. Theory Comput.*, 2017, **13**, 4467–4481.
14 M. Chaplin, *Nat. Rev. Mol. Cell Biol.*, 2006, **7**, 861–866.
15 M.-C. Bellissent-Funel, A. Hassanali, M. Havenith, R. Henchman, P. Pohl, F. Sterpone, D. van der Spoel, Y. Xu and A. E. Garcia, *Chem. Rev.*, 2016, **116**, 7673–7697.
16 D. Laage, T. Elsaesser and J. T. Hynes, *Chem. Rev.*, 2017, **117**, 10694–10725.
17 P. Setny, R. Baron, P. M. Kekenes-Huskey, J. A. McCammon and J. Dzubiella, *Proc. Natl. Acad. Sci. U. S. A.*, 2013, **110**, 1197–1202.
18 R. Godawat, S. N. Jamadagni and S. Garde, *Proc. Natl. Acad. Sci. U. S. A.*, 2009, **106**, 15119–15124.
19 R. Baron, P. Setny and J. A. McCammon, *J. Am. Chem. Soc.*, 2010, **132**, 12091–12097.

20 J. C. Smith, S. Cusack, U. Pezzeca, B. Brooks and M. Karplus, *J. Chem. Phys.*, 1986, **85**, 3636–3654.
21 T. Ichiye and M. Karplus, *Proteins*, 1991, **11**, 205–217.
22 L. Hong, N. Jain, X. Cheng, A. Bernal, M. Tyagi and J. C. Smith, *Sci. Adv.*, 2016, **2**, e1600886.
23 A. Orecchini, A. Paciaroni, A. D. Francesco, C. Petrillo and F. Sacchetti, *J. Am. Chem. Soc.*, 2009, **131**, 4664–4669.
24 M. Heyden and D. J. Tobias, *Phys. Rev. Lett.*, 2013, **111**, 218101.
25 V. Conti Nibali, G. D'Angelo, A. Paciaroni, D. J. Tobias and M. Tarek, *J. Phys. Chem. Lett.*, 2014, **5**, 1181–1186.
26 M. Heyden, *J. Chem. Phys.*, 2014, **141**, 22D509.
27 L. U. L. Brinkmann and J. S. Hub, *Proc. Natl. Acad. Sci. U. S. A.*, 2016, **113**, 10565–10570.
28 K. Moritsugu, A. Kidera and J. C. Smith, *J. Phys. Chem. B*, 2014, **118**, 8559–8565.
29 T. R. M. Barends, L. Foucar, A. Ardevol, K. Nass, A. Aquila, S. Botha, R. B. Doak, K. Falahati, E. Hartmann, M. Hilpert, M. Heinz, M. C. Hoffmann, J. Köfinger, J. E. Koglin, G. Kovacsova, M. Liang, D. Milathianaki, H. T. Lemke, J. Reinstein, C. M. Roome, R. L. Shoeman, G. J. Williams, I. Burghardt, G. Hummer, S. Boutet and I. Schlichting, *Science*, 2015, **350**, 445–450.
30 D. Russo, A. Laloni, A. Filabozzi and M. Heyden, *Proc. Natl. Acad. Sci. U. S. A.*, 2017, **114**, 11410–11415.
31 S. H. Chen, C. Y. Liao, H. W. Huang, T. M. Weiss, M. C. Bellisent-Funel and F. Sette, *Phys. Rev. Lett.*, 2001, **86**, 740–743.
32 M. C. Rheinstädter, C. Ollinger, G. Fragneto, F. Demmel and T. Salditt, *Phys. Rev. Lett.*, 2004, **93**, 108107.
33 M. C. Rheinstädter, T. Seydel and T. Salditt, *Phys. Rev. E: Stat., Nonlinear, Soft Matter Phys.*, 2007, **75**, 011907.
34 J.-P. Cartailler, H. Haigler and H. Luecke, *Biochemistry*, 2000, **39**, 2475–2483.
35 J. P. M. Jämbeck and A. P. Lyubartsev, *J. Chem. Theory Comput.*, 2012, **8**, 2938–2948.
36 C.-Y. Cheng, J. Varkey, M. R. Ambroso, R. Langen and S. Han, *Proc. Natl. Acad. Sci. U. S. A.*, 2013, **110**, 16838–16843.
37 M. J. Abraham, T. Murtola, R. Schulz, S. Páll, J. C. Smith, B. Hess and E. Lindahl, *SoftwareX*, 2015, **1**, 19–25.
38 V. Hornak, R. Abel, A. Okur, B. Strockbine, A. Roitberg and C. Simmerling, *Proteins: Struct., Funct., Bioinf.*, 2006, **65**, 712–725.
39 R. B. Best and G. Hummer, *J. Phys. Chem. B*, 2009, **113**, 9004–9015.
40 K. Lindorff-Larsen, S. Piana, K. Palmo, P. Maragakis, J. L. Klepeis, R. O. Dror and D. E. Shaw, *Proteins*, 2010, **78**, 1950–1958.
41 A. E. Aliev, M. Kulke, H. S. Khaneja, V. Chudasama, T. D. Sheppard and R. M. Lanigan, *Proteins*, 2014, **82**, 195–215.
42 J. P. M. Jämbeck and A. P. Lyubartsev, *J. Phys. Chem. B*, 2012, **116**, 3164–3179.
43 J. L. Abascal and C. Vega, *J. Chem. Phys.*, 2005, **123**, 234505.
44 S. Miyamoto and P. A. Kollman, *J. Comput. Chem.*, 1992, **13**, 952–962.
45 B. Hess, *J. Chem. Theory Comput.*, 2008, **4**, 116–122.
46 S. Páll and B. Hess, *Comput. Phys. Commun.*, 2013, **184**, 2641–2650.
47 T. Darden, D. York and L. Pedersen, *J. Chem. Phys.*, 1993, **98**, 10089–10092.
48 U. Essmann, L. Perera, M. L. Berkowitz, T. Darden, H. Lee and L. G. Pedersen, *J. Chem. Phys.*, 1995, **103**, 8577–8593.
49 G. Bussi, D. Donadio and M. Parrinello, *J. Chem. Phys.*, 2007, **126**, 014101.
50 H. Berendsen, J. Postma, W. van Gunsteren, A. DiNola and J. Haak, *J. Chem. Phys.*, 1984, **81**, 3684–3690.
51 M. Heyden, J. Sun, S. Funkner, G. Mathias, H. Forbert, M. Havenith and D. Marx, *Proc. Natl. Acad. Sci. U. S. A.*, 2010, **107**, 12068–12073.
52 A. Rahman and F. H. Stillinger, *Phys. Rev. A: At., Mol., Opt. Phys.*, 1974, **10**, 368.
53 F. Sciortino and S. Sastry, *J. Chem. Phys.*, 1994, **100**, 3881–3893.
54 M. Tarek and D. J. Tobias, *Phys. Rev. Lett.*, 2002, **88**, 138101.
55 F. Sterpone, G. Stirnemann and D. Laage, *J. Am. Chem. Soc.*, 2012, **134**, 4116–4119.
56 J. T. King, E. J. Arthur, C. L. Brooks and K. J. Kubarych, *J. Am. Chem. Soc.*, 2014, **136**, 188–194.
57 F. Sette, G. Ruocco, M. Krisch, C. Masciovecchio, R. Verbeni and U. Bergmann, *Phys. Rev. Lett.*, 1996, **77**, 83–86.
58 S. Saito and B. Bagchi, *J. Chem. Phys.*, 2019, **150**, 054502.
59 S. N. Jamadagni, R. Godawat and S. Garde, *Annu. Rev. Chem. Biomol. Eng.*, 2011, **2**, 147–171.
60 E. Lindahl and O. Edholm, *Biophys. J.*, 2000, **79**, 426–433.